

# Reversible Breaking and Forming of Metal–Ligand Coordination Bonds: Temperature-Triggered Single-Crystal to Single-Crystal Transformation in a Metal–Organic Framework

María C. Bernini,<sup>[b]</sup> Felipe Gándara,<sup>[a]</sup> Marta Iglesias,<sup>[a]</sup> Natalia Snejko,<sup>[a]</sup> Enrique Gutiérrez-Puebla,<sup>[a]</sup> Elena V. Brusau,<sup>[b]</sup> Griselda E. Narda,<sup>[b]</sup> and M. Ángeles Monge<sup>\*[a]</sup>

**Abstract:** [Yb(C<sub>4</sub>H<sub>4</sub>O<sub>4</sub>)<sub>1.5</sub>] undergoes a temperature-triggered single-crystal to single-crystal transformation. Thermal X-ray single-crystal studies showed a reversibly orchestrated rearrangement of the atoms generated by the breaking/formation of coordination bonds, in which the stoichiometry of the compound remains unchanged. The transformation occurs on heating the crystal

at ≈130 °C. This uncommon behavior was also studied by thermal methods, FTIR spectroscopy, and thermodiffraction. Both polymorphs, **α** (room-

**Keywords:** heterogeneous catalysis • metal–organic frameworks • polymorphism • structure elucidation • ytterbium

temperature form) and **β** (high-temperature form), are proven to be active heterogeneous catalysts; the higher catalytic activity of **β** is owed to a decrease in the Yb coordination number. A mechanism based on spectroscopic evidence and involving formation of the active species Yb–O–OH is proposed for the sulfide oxidation.

## Introduction


Metal–organic frameworks (MOFs) continue to attract much attention because of their interesting structural chemistry and their potential applications, among which are

catalysis, adsorption processes (gas storage), luminescence, and magnetism.<sup>[1–6]</sup> A key step for the construction of such materials is to select not only the experimental synthesis conditions, but also the appropriate multidentate bridging ligands. There has been much interest in aliphatic dicarboxylates because of their varied coordination modes and flexibility, which generally favor the development of three-dimensional networks. Rare-earth succinates have been studied widely and several inorganic–organic frameworks have been obtained and characterized.<sup>[3,7–14]</sup> Although the properties of the rare-earth element and the flexible succinate anion are combined in these frameworks, the properties of the compounds such as luminescence<sup>[8,14,15]</sup> or catalysis<sup>[3]</sup> have been evaluated in only a few studies.

However, the transformations of one hybrid polymeric structure to another are rare in solid-state supramolecular reactions as the breaking and formation of bonds should occur in more than one direction simultaneously. Most of the reversible topotactic solid-state reactions involve the removal of guest solvent molecules from cavities.<sup>[16]</sup> Although single-crystal to single-crystal transformations have received considerable attention in crystal engineering, only limited examples are known, since it is difficult for crystals to retain single crystallinity after the solid-state rearrangement of atoms.<sup>[17]</sup> The driving forces of such processes are varied—

[a] F. Gándara, Dr. M. Iglesias, Dr. N. Snejko, Prof. E. Gutiérrez-Puebla, Prof. M. Á. Monge  
Department of Structure and Synthesis of Oxides  
Instituto de Ciencia de Materiales de Madrid–CSIC  
C/Sor Juana Inés de la Cruz 3, 28049 Madrid (Spain)  
Fax: (+34) 913-720-623  
E-mail: amonge@icmm.csic.es

[b] M. C. Bernini, Dr. E. V. Brusau, Dr. G. E. Narda  
Area de Química General e Inorgánica "Dr. G. F. Puelles"  
Facultad de Química, Bioquímica y Farmacia  
Chacabuco y Pedernera  
Universidad Nacional de San Luis  
5700 San Luis (Argentina)

 Supporting Information (complete assignment of the infrared spectra of the [Yb(C<sub>4</sub>H<sub>4</sub>O<sub>4</sub>)<sub>1.5</sub>] polymorphs for this article is available on the WWW under <http://dx.doi.org/10.1002/chem.200802385>. CCDC-706459 (**α** polymorph at 296 K), -706460 (**α** polymorph at 374 K), -706461 (**β** polymorph at 408 K), -706462 (**β** polymorph at 429 K), and -706463 (**α** polymorph at 293 K after heating) contain the supplementary crystallographic data for this paper. These data can be obtained free of charge from The Cambridge Crystallographic Data Centre via [www.ccdc.cam.ac.uk/data\\_request/cif](http://www.ccdc.cam.ac.uk/data_request/cif).

for example: a) sorption/desorption of guest molecules induced by vacuum or temperature changes;<sup>[18]</sup> b) light;<sup>[19]</sup> c) rearrangement of solvent molecules;<sup>[20]</sup> d) a decrease in temperature;<sup>[21,22]</sup> e) an increase in temperature.<sup>[18b,23]</sup> The single-crystal to single-crystal transformation described in this report is unusual since it differs from the systems mentioned above in two important aspects: that it consists of a reversibly orchestrated rearrangement of the atoms generated by the breaking/formation of coordination bonds, this case being one of the few in which the stoichiometry of the compound is preserved; and that the single-crystal to single-crystal phase transition occurs when the crystal is heated at  $\approx 130^\circ\text{C}$ , whereas the only reversible process yet reported in MOFs takes place on cooling.<sup>[22]</sup>

Here, we present the synthesis and a complete single-crystal structural study of the thermal hysteresis cycle at 23, 100, 135, 156, and  $20^\circ\text{C}$  of a novel ytterbium succinate. The study includes variable-temperature IR spectroscopy, and variable-temperature powder XRD of the ytterbium succinate in its two polymorphic forms: the  $\alpha$  polymorph, at room temperature; and the  $\beta$  polymorph, at high temperature. The catalytic activity of the  $\alpha$  polymorph has been evaluated in reactions such as oxidation of methylsulfanylbenzene, acetalization of benzaldehyde, or hydrodesulfurization of thiophene. This last reaction was selected to correlate the structural differences of the two polymorphs with their catalytic activities.

## Results and Discussion

**Description and characterization of the two polymorphic structures:** A new crystalline compound is formed during the hydrothermal reaction of ytterbium nitrate with succinic acid. From its crystal structure, we found the formula to be  $[\text{Yb}(\text{C}_4\text{H}_4\text{O}_4)_{1.5}]$ . As explained below, this new compound may exist in two polymorphic phases, with reversible transitions from one to the other through temperature changes. The room-temperature phase crystallizes in the triclinic space group  $P\bar{1}$ . In this structure each metal is surrounded by eight oxygen atoms, all from carboxylate groups (see Figure 1a). The Yb coordination sphere in the  $\alpha$  polymorph forms a  $\text{YbO}_8$  triangulated dodecahedron. Yb–O bond lengths are in the range 2.215(6)–2.530(6) Å, which is consistent with that of previously reported carboxylate-containing ytterbium complexes.<sup>[24]</sup>

$\text{YbO}_8$  polyhedra are linked together by sharing edges, giving rise to chains that run in a zigzag along the  $a$  direction (Figures 2a and 3a). These chains are connected by two crystallographically nonequivalent succinate anions along the  $b$  and  $c$  directions, giving a 3D hybrid framework of the  $\text{I}^1\text{O}^2$  type, according to the classification proposed by Rao et al.<sup>[6]</sup> The chains of polyhedra are connected along the  $c$  direction by succinate anions in a perfect *trans* conformation (torsional angle =  $180.0^\circ$ ; distance between the  $\alpha$ - and  $\omega$ -carbon atoms = 3.875(12) Å). Both carboxylate groups of the *trans*-succinate anion are linked in a  $\eta_2\mu_3$ - $\eta_2\mu_3$  chelate-

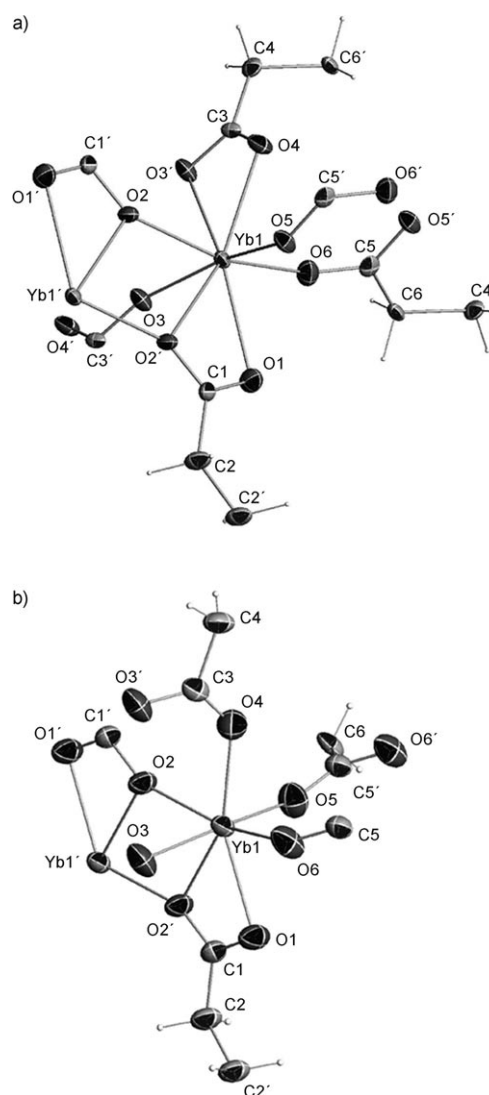


Figure 1. Coordination sphere of  $\text{Yb}^{\text{III}}$  ion in a) the  $\alpha$  polymorph; b) the  $\beta$  polymorph.

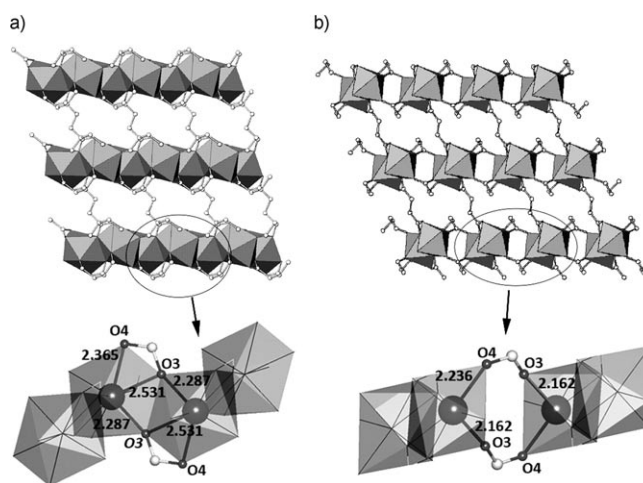


Figure 2. Projection on the  $ac$  plane of a) the  $\alpha$  polymorph; b) the  $\beta$  polymorph.

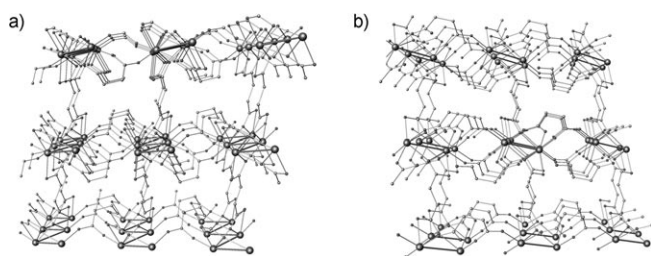


Figure 3. Perspective view along the (1,0,0) direction of a) the  $\alpha$  polymorph; b) the  $\beta$  polymorph.

bridge mode. In this way, the O2 atom connects two Yb ions at 2.260(6) and 2.425(6) Å. In the *b* direction (see Figure 3a) the chains are linked by a  $\eta_2\mu_2$  bidentate-bridge carboxylate group from a succinate anion in a *gauche* conformation (torsional angle =  $-75.5^\circ$ ; distance between the  $\alpha$ - and  $\omega$ -carbon atoms = 3.208(12) Å). The *gauche* isomer, acting as a  $\eta_2\mu_2$ - $\eta_2\mu_3$  linker, has the O3 oxygen atom bonded to two Yb atoms at distances of 2.287(6) and 2.530(6) Å. Thus, the carboxylate groups in both types of chelate bridge in the different conformers are involved in the development of the polyhedron chains. This explains why the distances between adjacent metal centers are not all equivalent, and it is possible to define two planes to identify the different distances. In the Yb–O2–Yb plane the distance between the metal centers is 3.877(1) Å and in the Yb–O3–Yb plane Yb...Yb = 4.013(1) Å. The two planes form an angle of approximately  $97.42^\circ$  in such a way that the Yb polyhedra are nearly perpendicular to each other.

The network can be described topologically as a three-nodal net. The Yb atoms are six-connected nodes, and the two different succinate anions are two different four-connected nodes. This network has the point (Schläfli) symbol  $(4^2.8^4)(4^4.6^2)_2(4^6.6^6)_2$ . However, the structure can be described more simply by considering the succinate anions just as linkers connecting the nodes located at the Yb atom positions. In this simpler representation, the zigzag chains of Yb polyhedra running along the *a* axis (as described above) are the secondary building units (SBUs). The chains are connected by the ligands along the *c* and *b* axes. From this depiction a uninodal net is defined in which each node is connected directly to two others in the same chain and to two other nodes in two different chains through the linkers, resulting in a four-connected network of the **dia** type (Figure 4a).

A weak endothermic signal not associated with weight change is observed in the differential thermal analysis (DTA) curve at  $130^\circ\text{C}$  (Figure 5). The organic part decomposes at  $410^\circ\text{C}$  with an experimental weight loss of 43.2% (expected value 44.4%); a sharp and intense exothermic peak in the DTA trace accounts for this process. The first DTA signal was investigated by differential scanning calorimetry (DSC) measurements in the ranges  $25$ – $190^\circ\text{C}$  and  $190$ – $25^\circ\text{C}$  (Figure 5, inset). The existence of measurable latent heat or a discontinuous volume change or hysteresis

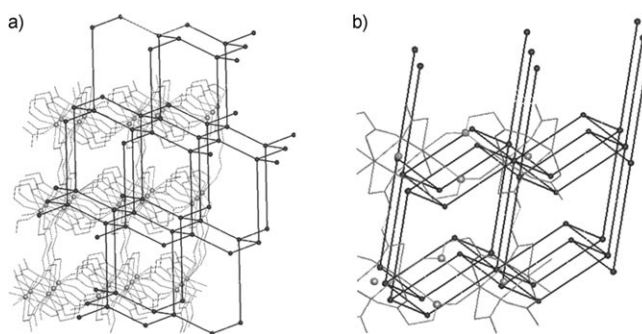


Figure 4. Topological depictions of: a) The  $\alpha$  polymorph in its maximum simplification as an uninodal net, with the **dia** topology; b) the  $\beta$  polymorph as a binodal net, with one of the succinate ligands as a three-connected node and the dimeric ytterbium units as the eight-connected center, resulting in a **tfz-d** topology.

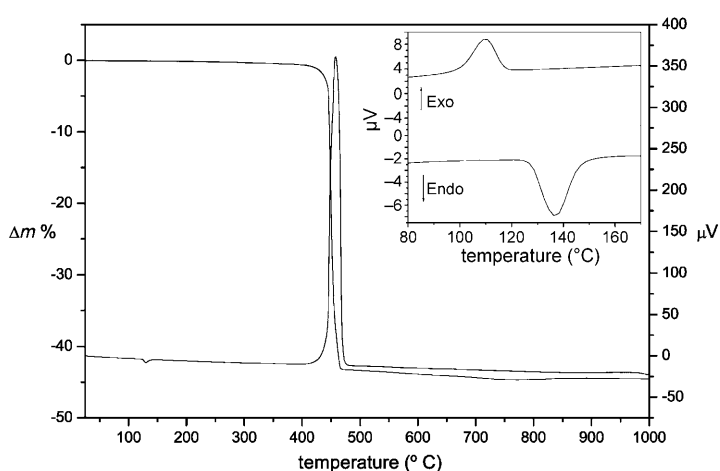


Figure 5. TGA/DTA curves of the new material. Inset: the DSC curves.

in the DSC curves may be taken as characteristic of a first-order transition,<sup>[25]</sup> in which the high-temperature phases with high internal energy will also have higher entropy.

Exploration of the possible structural changes associated with this transition by X-ray powder thermodiffraction (XRTD; Figure 6) revealed a reversible phase transition occurring when the sample was heated above  $130^\circ\text{C}$ , the initial structure being recovered when the sample returned to room temperature. The cell parameters of the high-temperature phase could be determined by indexing the X-ray powder pattern, employing the program DICVOL04,<sup>[26]</sup> included in the Fullprof Suite software package.<sup>[27]</sup> A solution was obtained in the triclinic system with cell parameters  $a = 6.45$  Å,  $b = 8.18$  Å,  $c = 8.62$  Å,  $\alpha = 92.84^\circ$ ,  $\beta = 110.21^\circ$ ,  $\gamma = 109.12^\circ$ , and cell volume =  $396.9$  Å<sup>3</sup> (figure of merit  $M(20) = 24.1$ ). As the phase transition occurs without loss of crystallinity in the sample, a variable-temperature single-crystal X-ray diffraction study was carried out. A single crystal of the  $\alpha$  polymorph was heated at  $156^\circ\text{C}$ . The cell parameters coincided with those obtained from the indexing of the powder pattern. Furthermore, the quality of the single crys-

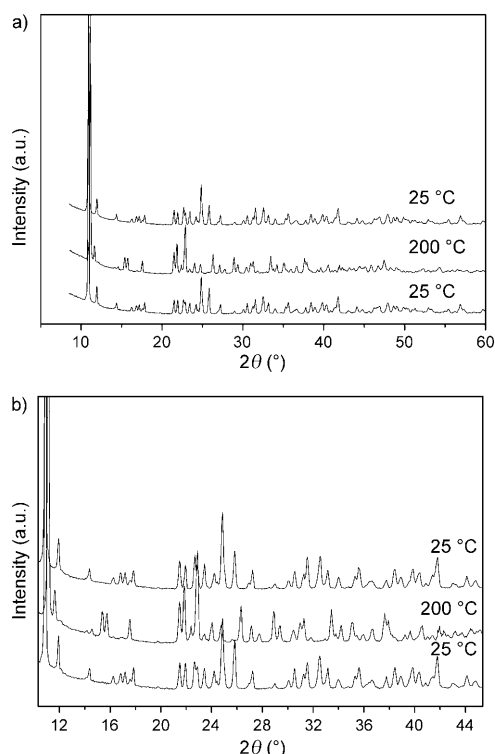


Figure 6. XRD powder patterns: a)  $2\theta = 8^\circ$ – $60^\circ$ ; b) zoomed in to  $2\theta = 10^\circ$ – $40^\circ$ . The patterns at  $25^\circ\text{C}$  correspond to the  $\alpha$  polymorph and the patterns at  $200^\circ\text{C}$  correspond to the  $\beta$  polymorph.

tal remained unaltered, allowing complete data to be collected for solution and refinement of the high-temperature structure. Subsequently, a complete structural study of the phase transition was achieved by examining the crystal at 23, 100, 135, and  $155^\circ\text{C}$  and again at  $20^\circ\text{C}$ . The main crystallographic and refinement data are given in Table 1, and bond lengths in the coordination spheres for both polymorphs at each temperature in Table 2.

The  $\beta$  polymorph also crystallizes in the triclinic space group  $P\bar{1}$ . In this structure each metal is surrounded by

Table 1. Main crystallographic data for polymorphs  $\alpha$  and  $\beta$  of  $[\text{Yb}(\text{C}_4\text{H}_4\text{O}_4)_{1.5}]$  at different temperatures.<sup>[a]</sup>

Polymorph	$\alpha$	$\alpha$	$\beta$	$\beta$	$\alpha$
temperature [K]	296	374	408	429	293 <sup>[b]</sup>
crystal system/space group/Z			triclinic / $P\bar{1}$ / 2		
<i>a</i> [Å]	5.9289(13)	5.9775(12)	6.4334(13)	6.4529(13)	5.9619(12)
<i>b</i> [Å]	8.0629(17)	8.1062(16)	8.1428(16)	8.1694(16)	8.0893(16)
<i>c</i> [Å]	8.6516(19)	8.6773(17)	8.5979(17)	8.6160(17)	8.6744(17)
$\alpha$ [°]	72.994(3)	73.13(3)	92.87(3)	92.79(3)	73.099(3)
$\beta$ [°]	72.959(3)	73.05(3)	110.20(3)	110.30(3)	73.144(3)
$\gamma$ [°]	69.464(3)	69.19(3)	108.98(3)	108.92(3)	69.326(3)
<i>V</i> [Å <sup>3</sup> ]	361.89(14)	367.69(13)	392.97(14)	396.27(14)	366.21(13)
reflections collected/unique with $I > 2\sigma(I)$	1668/1425	1714/1463	1838/1499	1854/1514	1700/1455
goodness-on-fit on $F^2$	0.989	1.037	0.985	0.995	1.002
<i>R</i> indices [ $I > 2\sigma(I)$ ]	$R_1 = 0.0397$ $wR_2 = 0.0756$	$R_1 = 0.0428$ $wR_2 = 0.1011$	$R_1 = 0.0422$ $wR_2 = 0.0952$	$R_1 = 0.0432$ $wR_2 = 0.0994$	$R_1 = 0.0298$ $wR_2 = 0.0666$

[a] Molecular weight =  $347.15 \text{ g mol}^{-1}$  [b] After heating.

Table 2. Bond lengths of coordination spheres of polymorphs  $\alpha$  and  $\beta$  at different temperatures.

Bond	Phase				
	$\alpha$ at RT	$\alpha$ at $100^\circ\text{C}$	$\beta$ at $135^\circ\text{C}$	$\beta$ at $155^\circ\text{C}$	$\alpha$ at RT after heating
Length [Å]					
Yb–O1	2.433(7)	2.444(7)	2.370(6)	2.380(7)	2.439(7)
Yb–O2	2.260(6)	2.266(7)	2.287(7)	2.280(6)	2.259(6)
Yb–O2 <sup>[a]</sup>	2.425(6)	2.444(6)	2.446(6)	2.454(6)	2.440(6)
Yb–O3	2.287(6)	2.287(7)	2.163(7)	2.162(7)	2.282(6)
Yb–O3 <sup>[b]</sup>	2.530(6)	2.545(7)	3.490 <sup>[c]</sup>	3.512 <sup>[c]</sup>	2.537(6)
Yb–O4	2.366(6)	2.346(7)	2.226(7)	2.236(7)	2.347(6)
Yb–O5	2.215(6)	2.201(7)	2.210(7)	2.212(7)	2.229(6)
Yb–O6	2.206(6)	2.201(7)	2.173(8)	2.180(7)	2.208(6)

[a] Symmetry transformations used to generate equivalent atoms:  $-x, -y + 1, -z + 1$ ; [b]  $-x + 1, -y + 1, -z + 1$ . [c] Not a bond.

seven oxygen atoms (see Figure 1b). The coordination sphere of  $\beta$  forms a  $\text{YbO}_7$  pentagonal bipyramid with Yb–O bond lengths in the range  $2.162(7)$ – $2.454(6)$  Å. The  $\text{YbO}_7$  polyhedra are joined, forming edge-sharing dimeric units (Figure 2b). These dimers are linked by two crystallographically nonequivalent succinate anions in the three spatial directions, leading to a type  $\text{I}^0\text{O}^3$  coordination polymer, according to the classification proposed by Rao et al.<sup>[6]</sup> The dimeric units in  $\beta$  are connected along the *c* direction by the  $\eta_2\mu_3$ – $\eta_2\mu_3$  succinate anions in a perfect *trans* conformation, in exactly the same way as in polymorph  $\alpha$ . However, along the *a* and *b* directions (see Figure 3b) the dimers in  $\beta$  are joined by the  $\eta_2\mu_2$ – $\eta_2\mu_2$  bidentate bridge carboxylate groups from the succinate anions in a *gauche* conformation (torsional angle:  $-79.4^\circ$ ; distance between the  $\alpha$ - and  $\omega$ -carbon atoms =  $3.255(13)$  Å). This change in the *gauche* ligand coordination mode from  $\eta_2\mu_3$ – $\eta_2\mu_2$  in the  $\alpha$  polymorph to  $\eta_2\mu_2$ – $\eta_2\mu_2$  in the  $\beta$  polymorph, together with the subsequent reduction in the Yb coordination number, creates the difference between the two polymorphs.

The cell volume of the  $\beta$  polymorph is about 10% greater than that of the  $\alpha$  form, mainly because the *a* parameter is higher. This is explained by the breaking of the Yb–O3' bond, and thus the rupture of the chains along the *a* direction to give the dimeric units (see Figures 1 and 2b). At higher temperatures, the molecular vibration acquires more energy and the *gauche* succinate conformer becomes more unstable because of the steric impediment. When the Yb–O3' bond is broken the *gauche* succinate can relax, changing the torsional angle from  $-75.5^\circ$  to  $-79.4^\circ$ . The O3 atom in the  $\beta$  polymorph is no longer shared by neighboring coordination polyhedra. The resulting SBUs after the phase transition are dimeric

units, with  $\text{Yb}\cdots\text{Yb}=3.931(1)\text{ \AA}$ , separated from one another by  $4.90\text{ \AA}$ .

The expected increment in the thermal factors with increasing temperature is verified from the structural analysis at the five selected temperatures. The mean square atomic displacements of the O3 atom (see Table 3) provide strong

Table 3. Principal mean square atomic displacements,  $U^2$ , for the O3 atom at different temperatures.

Temperature [°C]	$U_x^2$	$U_y^2$	$U_z^2$	$\Delta(U_x^2)$	$\Delta(U_y^2)$	$\Delta(U_z^2)$
23	0.0284	0.0192	0.0114			
				0.0133	0.0057	0.0028
100	0.0417	0.0249	0.0142			
				0.0258	0.0126	0.0102
135	0.0615	0.0375	0.0244			
				0.0058	0.0061	0.0008
155	0.0673	0.0436	0.0252			
				-0.0319	-0.0211	-0.0132
20 <sup>[a]</sup>	0.0354	0.0255	0.0120			

[a] After heating.

evidence for this. It is striking that the major increment occurs not with the greatest jump in temperature, but between 100 and  $135^\circ\text{C}$  (see  $\Delta U^2_i$  in Table 3). Furthermore, the major increase is associated with the  $x$  component of the thermal ellipsoid. This surely explains the breakage of the  $\text{Yb}-\text{O}3'$  bond at  $\approx 130^\circ\text{C}$  and consequently the observed phase transition with the elongation of the  $a$  parameter as the main structural cell change. It is noteworthy that upon return to RT, when the  $\text{Yb}-\text{O}3$  bond is formed again, the thermal parameter  $U_x^2$  in the  $a$  direction nearly recovers its original value (Table 3).

The new network cannot be depicted topologically on the basis of a rod-shaped SBU, as in the room-temperature polymorph. In this new net, a node is the dimeric unit of the Yb polyhedra. The *trans*-succinate is a linker between two of these nodes, and now the *gauche* succinate should be considered as a three-connected center. As a result, the  $\beta$  polymorph exhibits a binodal network, eight- and three-connected, of the **tfz-d** type (see Figure 4b), with total point (Schläfli) symbol  $(4^3)_2(4^6.6^{18}.8^4)$ .

Variable-temperature IR spectroscopy was used to correlate the structural changes and thermal vibrations with the IR spectra. The IR spectra were interpreted by considering the internal vibrations of carboxylate and methylene groups and comparing them with those observed in succinic acid, similar compounds, and related data in the literature.<sup>[9,28,29]</sup> The complete assignment of the spectra of both polymorphs is tabulated in the Supporting Information. The IR spectra of both polymorphs display the antisymmetric  $\tilde{\nu}_{\text{asym}}(\text{OCO})$  stretching mode in the  $1610\text{--}1550\text{ cm}^{-1}$  range as a broad band that includes two components (see Figure 7). This splitting into two bands can be explained in terms of the different coordination modes (chelate bridge and bidentate bridge) of the carboxylate groups in the polymorphs. The band corresponding to the symmetric  $\tilde{\nu}_{\text{sym}}(\text{OCO})$  stretching mode was assigned in both spectra at  $\approx 1400\text{ cm}^{-1}$  according

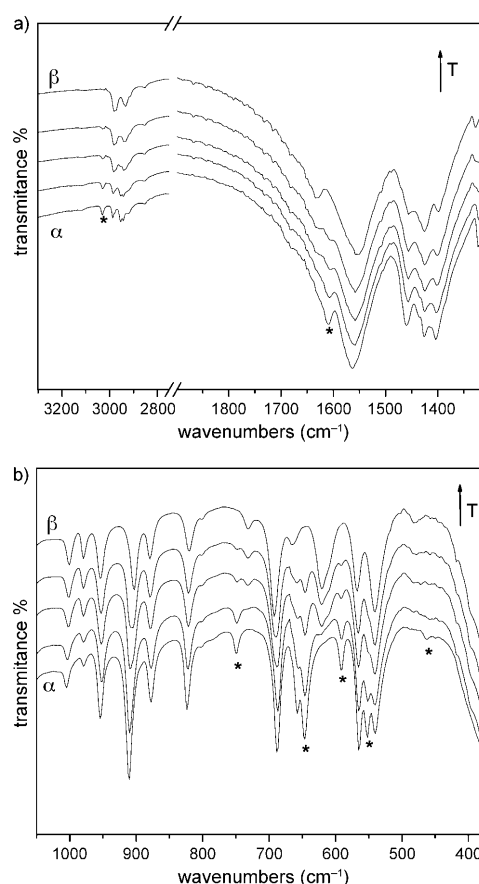
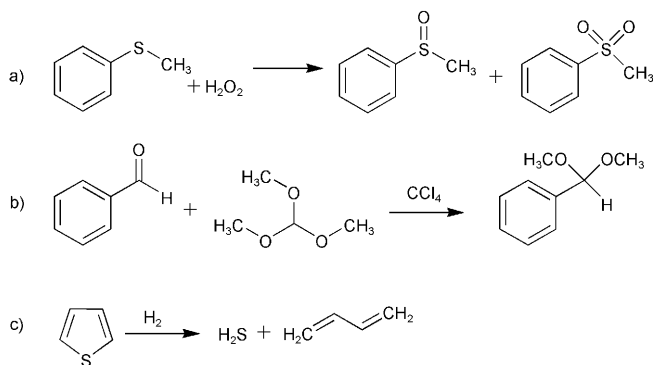


Figure 7. Variable-temperature IR spectra, showing the transition from the  $\alpha$  polymorph (a) to the  $\beta$  polymorph (b).

to an exhaustive IR study performed on a holmium succinate framework.<sup>[28]</sup> The  $\delta(\text{CH}_2)$  mode appears in the spectra in the  $1460\text{--}1425\text{ cm}^{-1}$  range as a strong band split into three components, of which the one at the highest frequency could be assigned to the bending mode of the *trans*-succinate anion whereas the two at lower frequency are tentatively assigned to the  $\delta(\text{CH}_2)$  mode of  $\text{CH}_2$  groups in the *gauche* succinate anion of each polymorph. The assignment of this mode took into account steric considerations explained in the vibrational study cited above. It is remarkable that certain bands are affected, as shown in Figure 7, by the structural changes associated with the phase transition, suggesting that the vibrational modes of  $\text{CH}_2$  and  $\text{OCO}$  groups in the *gauche* succinate anion could be related to those bands. This relationship is in complete agreement with the variation in the torsional angle and mode of coordination observed for this anion. Furthermore, the changes in the stretching  $\tilde{\nu}(\text{Yb}-\text{O})$  region allow us to assign the band at  $550\text{ cm}^{-1}$  to the  $\text{Yb}-\text{O}3$  stretching mode since it disappears progressively with increasing temperature and it is absent in the spectrum of the  $\beta$  polymorph. On the other hand, the band at  $460\text{ cm}^{-1}$ , which is assigned to the  $\text{Yb}-\text{O}$  stretching mode, undergoes a slight shift to higher frequencies consistent with the reinforcement that some  $\text{Yb}-\text{O}$  bonds experi-

ence (see Table 2). Asterisks in Figure 7 mark the principal differences between the spectra of the two polymorphs.

**Catalytic activity:** To test the catalytic activity of the new Yb succinate polymeric frameworks, they have been employed as heterogeneous catalysts in different types of reactions. The  $\alpha$  polymorph has been tested as a Lewis acid catalyst in the acetalization of aldehydes, and as a redox catalyst in the oxidation of sulfides (see Scheme 1). These reactions



Scheme 1. a) Oxidation of methylsulfanylbenezene; b) acetalization of aldehydes; c) hydrodesulfurization of thiophene.

not only constitute attractive and important methods in organic chemistry, but also participate in relevant green chemistry processes or play key roles in the activation of enzymes.<sup>[30]</sup> Although lanthanides are receiving increasing attention in the literature, they have scarcely been explored. Recently we reported catalytic activity for a series of rare earth MOFs in the methylsulfanylbenezene oxidation.<sup>[31]</sup> The Yb succinate  $\alpha$  polymorph behaves as heterogeneous catalyst, but the low temperatures at which these two reactions are carried out (see Experimental Section) make it impossible to evaluate the catalytic activity of the  $\beta$  polymorph, which exists only above 130 °C. Since the active metallic centers in the two polymorphs have different coordination numbers, a difference in the corresponding catalytic activity is expected. The hydrodesulfurization of thiophene was chosen to evaluate this difference, since it can occur at temperatures at which the two polymorphs could exist and act as heterogeneous catalysts.

**Acetalization of aldehydes:** The formation of acetals is one of the more effective and frequently used methods of protecting carbonyl groups.<sup>[32]</sup> Numerous studies exist of synthesis, protection, and masking of carbonyl groups, because acetals have great importance due to their roles both as intermediates of reaction and as final products.<sup>[33–36]</sup> The reaction of benzaldehyde with trimethyl orthoformate (TMOF) in the presence of the  $\alpha$  polymorph produces the corresponding dimethyl acetal in very good yield (90%), in a short reaction time (5 h), and under mild conditions (60 °C), indicating that benzaldehyde was protected successfully employing the new compound as catalyst (see Figure 8). Whereas most

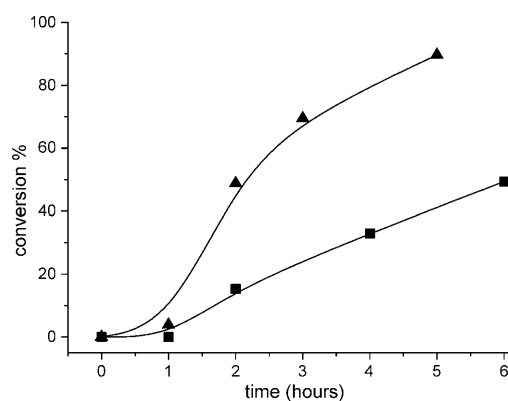


Figure 8. Kinetic curves for acetalization of benzaldehyde (▲) and for oxidation of methylsulfanylbenezene (■), with the  $\alpha$  polymorph as catalyst.

Lewis acids decompose or become deactivated in the presence of water, the new Lewis heterogeneous catalyst is stable both in water and in organic solvents. The TOF (turn-over frequency;  $2700 \text{ min}^{-1}$ ), indicating how often the substrate interacts with the catalyst, was calculated from the kinetic curves and is in agreement with the final conversion reached.

**Oxidation of sulfide:** The selective oxidation of sulfides to sulfoxides is an attractive and important method in organic chemistry since sulfoxides are useful building blocks, especially as chiral auxiliaries in organic synthesis.<sup>[37]</sup> They also play key roles in the activation of enzymes.<sup>[30]</sup> They have been synthesized from the corresponding sulfides by a wide range of oxidizing systems. Aqueous hydrogen peroxide is a particularly attractive oxidant since it is cheap, environmentally friendly, and easy to handle, and it produces water as the only by-product, thus reducing purification requirements.<sup>[38]</sup> The  $\alpha$  polymorph was tested as a redox catalyst in the oxidation of methylsulfanylbenezene with  $\text{H}_2\text{O}_2$  as the oxygen source, which was always in excess (10%) relative to the amount of substrate. The products of reaction at 60 °C were identified by GC. The results are summarized in Figure 8. The employment of 1.5 equiv of  $\text{H}_2\text{O}_2$  and its controlled addition allowed a significant improvement of the chemoselectivity of the process, and sulfoxide was obtained as the only product (selectivity = 92%). The new material was efficient and catalyzed selective sulfoxide formation under mild conditions, with a good yield (50%, TOF =  $457 \text{ min}^{-1}$ ) after 6 h of reaction.

**Recycling experiment:** In spite of the activation of the catalyst, an induction period of 1 h was observed in the oxidation reaction. We therefore performed a recycling experiment to investigate the behavior in later reaction cycles. Furthermore, this test gives us information about the stability of the catalyst. A marked increase in the activity is observed from the first to the second cycle of reaction, and a new minor increase takes place from the second toward the third cycle (Figure 9). Induction periods were not observed

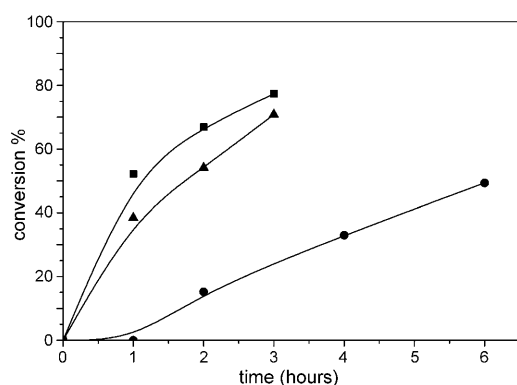


Figure 9. Kinetic curves for three consecutive cycles of oxidation of methylsulfanylbenezene with the  $\alpha$  polymorph as catalyst:  $\bullet$ : cycle 1;  $\blacktriangle$ : cycle 2;  $\blacksquare$ : cycle 3.

in the second and third reaction cycles. After this procedure, the catalyst was recovered by filtration, and then characterized by X-ray powder diffraction (XRPD) and IR spectroscopy (Figure 10). The corresponding powder pattern confirms that the compound acts as a heterogeneous catalyst since the structure is not affected by the reaction cycles. However, several bands appear in the IR spectrum (marked with asterisks, Figure 10, right). The band at  $1090\text{ cm}^{-1}$  had been found previously in the oxidation of methylsulfanylbenezene using other Ln-based MOFs that we reported recently.<sup>[31]</sup> In the present case, three additional new bands appear at 785, 530, and  $504\text{ cm}^{-1}$ . Notably, the last two bands are found in the Ln–O stretching zone.<sup>[39,40]</sup> This result supports the hypothesis that a Ln–O–OH species is formed during the first reaction cycle and behaves as the real active intermediate in the catalytic reaction. This would explain the increase in activity observed after the first reaction cycle. A possible reaction pathway is depicted in Scheme 2.

**Hydrodesulfurization of thiophene:** Elimination of organic sulfur compounds is an important process in green chemistry, and of special interest for the petrochemical industry. In the hydrodesulfurization (HDS), the thiophene decomposes to hydrogen sulfide and 1,3-butadiene, under a hydrogen atmosphere (Scheme 1c). Traditionally, Co–Mo-based catalysts are the most often employed in this reaction. As an alternative, we have recently evaluated the activity of hybrid organic–inorganic materials with ytterbium as the active

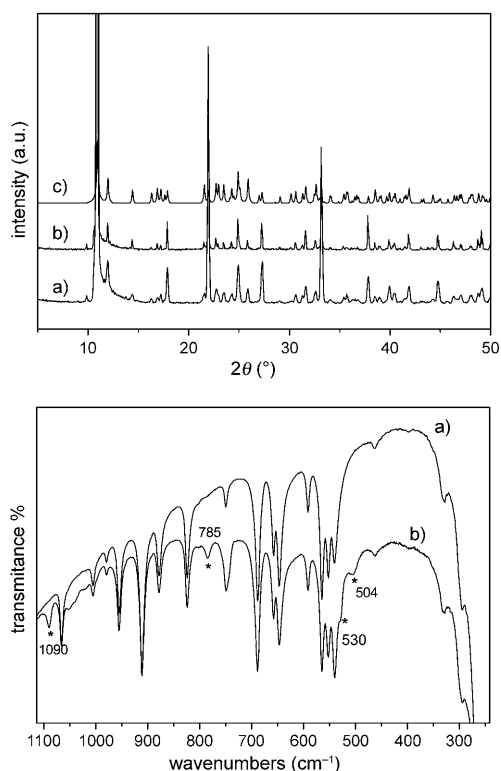
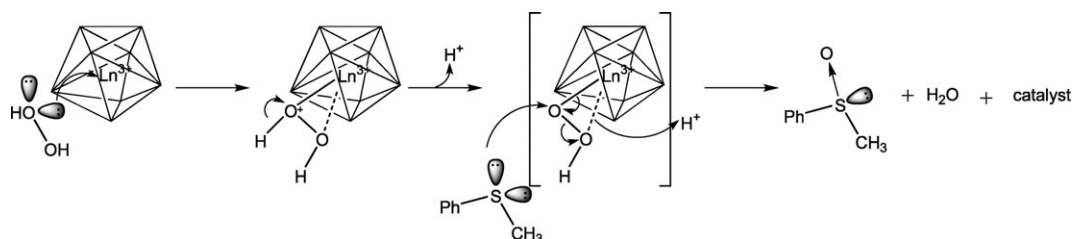


Figure 10. Top: X-ray powder diffraction patterns of the  $\alpha$  polymorph a) before and b) after three cycles of oxidation of methylsulfanylbenezene; c) simulated XRD powder pattern from the single-crystal XRD data. Bottom: IR spectra of the  $\alpha$  polymorph a) before and b) after three cycles of oxidation of methylsulfanylbenezene. The asterisks indicate the new bands in the spectra after the catalytic cycles.

center;<sup>[41]</sup> they were demonstrated to be able to reach very good yields of conversion, working at lower temperatures than the traditional catalysts. In the current study, the new Yb succinate has been employed as catalyst in the HDS of thiophene at different temperatures, to evaluate the influence of the structure, and therefore of the coordination environment of the metal, on the catalytic activity. Thus, from the percentage of thiophene decomposition after 4 h of heating under an  $\text{H}_2$  atmosphere (Figure 11), it is seen how the activity increases linearly with the temperature as expected. However, a change in the linear trend is observed between 120 and  $130^\circ\text{C}$ , returning to a good linear fit of the subsequent points. This change is associated with the phase transition suffered by the catalyst, and the greater slope of



Scheme 2. Proposed mechanism for the catalytic oxidation of methylsulfanylbenezene.



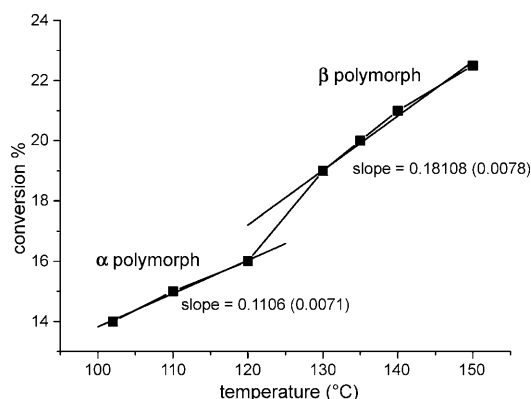


Figure 11. Differences in the linear trends observed in the hydrodesulfurization of thiophene.

the fitted line beyond this change indicates a higher activity of the  $\beta$  polymorph. This is due not only to the lower Yb coordination number in  $\beta$ , but also to the unhindered accessibility of the active sites to the reactants. Structurally speaking, the breaking of one Yb–O bond per Yb atom which accompanies the structural transformation is opening the gate to the reactants. Finally at 150 °C a good conversion of 68 % is achieved after 18 h of heating.

## Conclusion

We have successfully prepared a novel Yb MOF, which exhibits a reversible temperature-induced room temperature–high temperature phase transition without losing or gaining any solvent or guest molecules, so the two phases are polymorphs. Variable-temperature single-crystal X-ray studies showed a reversibly orchestrated rearrangement of the atoms generated by the breaking/formation of Yb–O bonds, in which the stoichiometry remains unchanged. The transformation from the  $\alpha$  to the  $\beta$  polymorph, which happens at 130 °C, involves the change of coordination number from eight to seven,  $[\text{YbO}_8]_n$  rod-shaped SBUs to  $[\text{YbO}_7]_2$  dimeric SBUs,  $\eta_2\mu_3\text{--}\eta_2\mu_2$  to  $\eta_2\mu_2\text{--}\eta_2\mu_2$  coordination in the *gauche* conformer of succinate, and a *dia*-type four-connected to a *tfa-d*-type binodal network, eight- and three-connected. The  $\alpha$  polymorph has proven to be an active acid and redox heterogeneous catalyst. The influence of the structure on the catalytic activity was tested in HDS of thiophene at different temperatures, which showed a higher activity for the  $\beta$  polymorph. Based on the spectroscopic evidence, a mechanism involving formation of the Ln–O–OH active species is proposed for the sulfide oxidation. This is, to our knowledge, the first reversible crystal-to-crystal phase transition in an MOF, in which the hysteresis cycle from one polymorph to the other goes from room temperature to high temperature: RT  $\rightarrow$  HT. Additional studies on these materials are ongoing to evaluate their optical and inclusion properties derived from the click of the Yb–O bond (opening/closing the gate).

## Experimental Section

**Synthesis:** All reagents were purchased at high purity (AR grade) from Merck (succinic acid) and Strem ( $\text{Yb}(\text{NO}_3)_3 \cdot 5\text{H}_2\text{O}$ ) and were used without further purification.

**$[\text{Yb}(\text{C}_4\text{H}_4\text{O}_4)_{1.5}]$  (polymorph  $\alpha$ ):** This compound was obtained by hydrothermal reaction of  $\text{Yb}(\text{NO}_3)_3 \cdot 5\text{H}_2\text{O}$  (1 mmol) with the ligand ( $\text{C}_4\text{H}_6\text{O}_4$  = succinic acid; 1.5 mmol) in water (5 mL) and adjusting the pH to 3.5 with triethylamine. The mixture of reagents was put in a Teflon-lined digestion bomb (internal volume 43 mL), heated at 180 °C for 90 h, and then cooled to RT. Prismatic colorless single crystals were collected after washing with distilled water and acetone.

**Crystal structure determination:** The cell parameters and the main data collection and refinement data for  $[\text{Yb}(\text{C}_4\text{H}_4\text{O}_4)_{1.5}]$  at the selected temperatures are summarized in Table 1. A suitable single crystal was mounted on a Bruker–Siemens Smart CCD diffractometer equipped with a normal focus, a 2.4 kW sealed-tube X-ray source ( $\text{MoK}_\alpha$  radiation,  $\lambda = 0.71073$  Å) operating at 40 kV and 30 mA. Data were collected over a hemisphere of reciprocal space by a combination of three sets of exposures. Each set had a different  $\theta$  angle for the crystal and each exposure of 20 s covered  $0.3^\circ$  in  $\omega$ . The crystal–detector distance was 5.5 cm. Coverage of the unique set was over 99 % complete to at least  $23^\circ$  in  $\theta$ . Unit cell dimensions were determined by a least-squares fit of 30 reflections and 20 s, with  $I > 20\sigma(I)$ . The first 100 frames of data were collected again at the end of the data collection process to monitor crystal decay. The intensities were corrected for Lorentz and polarization effects. Scattering factors for neutral atoms and anomalous dispersion corrections for Yb, O, and C were taken from the International Tables for Crystallography.<sup>[42]</sup> The structure was solved by direct methods and refined in the triclinic space group  $P\bar{1}$ . Full matrix least-squares refinement with anisotropic thermal parameters for all non-hydrogen atoms was carried out by minimizing  $\omega(F_o^2 - F_c^2)^2$ . Refinement on  $F^2$  for all reflections, weighted  $R$  factors ( $R_w$ ), and all goodness-of-fits  $S$  are based on  $F^2$ , while conventional  $R$  factors are based on  $F$ .  $R$  factors based on  $F^2$  are statistically about twice those based on  $F$ , and  $R$  factors based on all the data would be even larger. The conditions for data collection are summarized in Table 1. The hydrogen atoms of the ligand were fixed at calculated positions using distance and angle constraints. All calculations were performed using SMART software for data collection, SAINT<sup>[43]</sup> for data reduction, SHELXTL<sup>[44]</sup> to resolve and refine the structure and to prepare material for publication, and ATOMS<sup>[45]</sup> for molecular graphics.

**Temperature-dependent single-crystal X-ray diffraction measurements:** Single-crystal X-ray diffraction intensities were collected at 101, 135, 156, and 20 °C on an Oxford Diffraction Gemini S diffractometer, employing graphite monochromated  $\text{MoK}_\alpha$  radiation ( $\lambda = 0.71073$  Å). All measurements were performed on the same single crystal and the stabilization time for each one was set at 1 h once the desired temperature was reached. The structures were solved and refined using the methods and procedures detailed above.

**Temperature-dependent X-ray powder diffraction:** This was carried out with a Bruker D8 Advance powder diffractometer using  $\text{CuK}_\alpha$  radiation ( $\lambda = 1.5418$  Å,  $U = 40$  kV,  $I = 30$  mA) equipped with an MRI wide-temperature-range oven-camera (–195 to 450 °C) mounted on a theta–theta goniometer. Data were scanned over the range  $2\theta = 8.5\text{--}60^\circ$  with  $2\theta$  step size =  $0.05^\circ$  and counting time = 1 s/step. The heating and cooling process was controlled by Eurotherm 2404. The sample heating rate was  $0.2^\circ\text{C min}^{-1}$  from RT (20 °C) to 200 °C.

**Vibrational characterization:** The IR spectra were recorded over 4000–225  $\text{cm}^{-1}$  by the KBr pellet technique with a Nicolet Protégé 460 spectrometer, employing a variable-temperature cell with 64 scans; spectral resolution was  $2\text{ cm}^{-1}$ .

**Thermal analysis:** Thermogravimetric and differential thermal analyses (TGA/DTA) were performed using a Seiko TG/DTA 320 apparatus in the range 25–1000 °C in an air flow at  $20\text{ mL min}^{-1}$  at a heating rate of  $10^\circ\text{C min}^{-1}$ . DSC at 25–190 °C (at  $10^\circ\text{C min}^{-1}$  with about 25 mg of sample) was performed in a Mettler TA3000 system equipped with a DSC30 unit.



## Catalytic reactions

**General procedure for acetalization of aldehydes with TMOF:** Catalyst (0.025 mmol) was added to a solution of the carbonyl compound (2.5 mmol) and TMOF (2.5 mmol) in tetrachloromethane (5 mL) in a 25 mL flask equipped with a magnetic stirrer at 60 °C. Samples were taken at intervals and the reaction products were analyzed by gas chromatography (GC) on a Hewlett-Packard 5890 II chromatograph with a  $\beta$ -DEX 325 capillary column, equipped with an MS detector.

**General procedure for oxidation of sulfides with hydrogen peroxide:** The catalyst (0.025 mmol) was activated by stirring it with hydrogen peroxide (1.5 mmol, 25%) for 1 h at 60 °C in a 25 mL flask equipped with a magnetic stirrer. The reactor with the activated catalyst was then charged with acetonitrile (5 mL) and the corresponding thioether (methylsulfanylbenzene or 2-ethylbutyl phenyl sulfide, 2.52 mmol) and  $\text{H}_2\text{O}_2$  (1.5 mmol, 25%) was added dropwise, while the whole suspension was heated at 60 °C. Samples were taken hourly and analyzed after filtration. Chemical yields of sulfoxides and sulfones were measured by GC as above.

Thiophene was hydrodesulfurized in a Parr reactor under  $\text{H}_2$  (6 bar). For thiophene decomposition, substrate (10 mL, 125 mmol) and catalyst (0.043 g, 0.125 mmol) were mixed and heated at various temperatures, with stirring. After the selected time intervals, the reactor was cooled, then opened, and the remaining thiophene was measured.

**Recycling experiments:** Polymorph  $\alpha$  was recycled by using it in several methylsulfanylbenzene oxidation reaction cycles. Before reuse, the solid was filtered from the reaction medium and washed with diethyl ether; then fresh substrate and solvent were added without further catalyst, for three consecutive experiments. To verify the heterogeneous nature of the catalytic reaction we investigated the residual activity of the supernatant solution after separation of the catalyst. To investigate potential leaching, the organic phase of a first run was separated from the solid (catalyst). New reagents were added to the clear filtrate, and the composition of the homogeneous reaction mixture was determined by GC. This mixture was treated as a standard catalytic experiment. After 6 h the composition was determined, and no reaction was observed, which excluded the presence of active catalytic species in solution.

## Acknowledgements

F.G. acknowledges an FPI fellowship from the Ministerio de Educación y Ciencia (MEC) and the Fondo Social Europeo from the EU. This work has been supported by the Spanish MCYT Project Mat 2007-60822, CTQ 2007-28909-E/BQU, and Consolider-Ingenio CSD2006-2001. The authors thank Laura Torre from the X-Ray Group in the Universidad de Oviedo, for the variable-temperature single-crystal data collections. Dr. M. J. Martínez-López is acknowledged for her assistance in the DSC measurements. G.E.N. is a member of Consejo Nacional de Investigaciones Científicas y Técnicas (CONICET) and M.C.B. acknowledges a CONICET fellowship.

- [1] J. Perles, M. Iglesias, M. A. Martín-Luengo, M. A. Monge, C. Ruiz-Valero, N. Snejko, *Chem. Mater.* **2005**, *17*, 5837.
- [2] M. Hirscher, B. Panella, *Scr. Mater.* **2007**, *56*, 809.
- [3] J. Perles, M. Iglesias, C. Ruiz-Valero, N. Snejko, *J. Mater. Chem.* **2004**, *14*, 2683.
- [4] W. Mori, T. Sato, T. Ohmura, C. N. Kato, T. Takei, *J. Solid State Chem.* **2005**, *178*, 2555.
- [5] A. K. Cheetham, C. N. R. Rao, R. K. Feller, *Chem. Commun.* **2006**, 4780.
- [6] C. N. R. Rao, A. K. Cheetham, A. Thirumurugan, *J. Phys. Condens. Matter* **2008**, *20*, 083202.
- [7] A. Seguatni, M. Fakhfakh, M. J. Vauley, N. Jouini, *J. Solid State Chem.* **2004**, *177*, 3402–3410.
- [8] a) Y. F. Zhou, F. L. Jiang, D. Q. Yuan, B. L. Wu, M. C. Hong, *J. Mol. Struct.* **2005**, *743*, 21–27; b) S. C. Manna, E. Zangrando, A. Bencini, C. Benelli, N. R. Chaudhuri, *Inorg. Chem.* **2006**, *45*, 9114–9122.

- [9] M. C. Bernini, E. V. Brusau, G. E. Narda, G. E. Echeverria, C. G. Pozzi, G. Punte, C. W. Lehmann, *Eur. J. Inorg. Chem.* **2007**, 684–693.
- [10] W. Nika, I. Pantenburg, G. Meyer, *Acta Crystallogr. Sect. E* **2004**, *61*, m138–m140.
- [11] F. Serpaggi, G. Ferey, *Microporous Mesoporous Mater.* **2002**, *217*, 569–570.
- [12] M. Fleck, Z. Kristallogr. NCS **2002**, *217*, 569–570.
- [13] F. Li, *Acta Crystallogr. Sect. E* **2007**, *63*, m840–m841.
- [14] H. T. Zhang, Y. Song, Y. X. Li, J. L. Zuo, S. Gao, X. Z. You, *Eur. J. Inorg. Chem.* **2005**, 766–772.
- [15] F. Serpaggi, G. Ferey, *Microporous Mesoporous Mater.* **1999**, *32*, 311–318.
- [16] a) S. Rabe, U. Muller, Z. Anorg. Allg. Chem. **1999**, *625*, 1367–1370J; b) C. J. Kepert, M. J. Rosseinsky, *Chem. Commun.* **1999**, 375–376; c) H. Li, M. Eddaoudi, M. O’Keeffe, O. M. Yaghi, *Nature* **1999**, *402*, 276–279; d) D. V. Soldatov, E. V. Grachev, J. A. Ripmeester, *Cryst. Growth Des.* **2002**, *2*, 401–408.
- [17] a) D. Ranford, J. J. Vittal, D. Q. Wu, *Angew. Chem.* **1998**, *110*, 1159–1162; *Angew. Chem. Int. Ed.* **1998**, *37*, 1114–1116; b) L. Iordanidis, M. G. Kanatzidis, *J. Am. Chem. Soc.* **2000**, *122*, 8319–8320; c) J. J. Vittal, X. D. Yang, *Cryst. Growth Des.* **2002**, *2*, 259–262; d) S. Kitagawa, R. Kitaura, S. Noro, *Angew. Chem.* **2004**, *116*, 2388–2430; *Angew. Chem. Int. Ed.* **2004**, *43*, 2334–2375; e) K. Biradha, Y. Hongo, M. Fujita, *Angew. Chem.* **2002**, *114*, 3545–3548; *Angew. Chem. Int. Ed.* **2002**, *41*, 3395–3398; f) A. Michaelides, S. Skoulou, *Cryst. Growth Des.* **2005**, *5*, 529–533; g) J. J. Vittal, *Coord. Chem. Rev.* **2007**, *251*, 1781–1795, and references herein.
- [18] a) Q. Wei, M. Nieuwenhuyzen, F. Meunier, C. Hardacre, S. L. James, *Dalton Trans.* **2004**, 1807–1811; b) P. S. Mukherjee, N. Lopez, A. M. Arif, F. Cervantes-Lee, J. C. Noveron, *Chem. Commun.* **2007**, 1433–1435; c) J. P. Zhang, Y. Y. Lin, W. X. Zhang, X. M. Chen, *J. Am. Chem. Soc.* **2005**, *127*, 14162–14163.
- [19] a) H. Konaka, L. P. Wu, M. Munakata, T. Kuroda-Sowa, M. Maekawa, Y. Suenaga, *Inorg. Chem.* **2003**, *42*, 1928–1934; b) G. Georgiev, L. R. MacGillivray, *Chem. Soc. Rev.* **2007**, *36*, 1239–1248.
- [20] M. H. Mir, J. J. Vittal, *Cryst. Growth Des.* **2008**, *8*, 1478–1480.
- [21] a) D. K. Kumar, D. A. Jose, A. Das, P. Dastidar, *Inorg. Chem.* **2005**, *44*, 6933–6935; b) S. Yahyaoui, W. Rekik, H. Naili, T. Mhiri, T. Bataille, *J. Solid State Chem.* **2007**, *180*, 3560–3570.
- [22] C. H. Hu, U. Englert, *Angew. Chem.* **2005**, *117*, 2321–2323; *Angew. Chem. Int. Ed.* **2005**, *44*, 2281–2283.
- [23] a) G. Mahmoudi, A. Morsali, *Cryst. Growth Des.* **2008**, *8*, 391–394; b) N. L. Toh, M. Nagarathinam, J. J. Vittal, *Angew. Chem.* **2005**, *117*, 2277–2281; *Angew. Chem. Int. Ed.* **2005**, *44*, 2237–2241.
- [24] N. Rahahlia, K. Alioune, A. Guehria-Laidoudi, S. Dahaoui, C. Lecomte, *Acta Crystallogr. Sect. E* **2006**, *62*, m2543–m2545.
- [25] C. N. R. Rao, K. J. Rao in *Phase Transitions in Solids: An Approach to the Study of the Chemistry and Physics of Solids*, McGraw-Hill, New York, **1978**, p. 17.
- [26] A. Boulitf, D. Louer, *J. Appl. Crystallogr.* **2004**, *37*, 724–731.
- [27] J. Rodriguez-Carvajal, *Physica B+C* **1993**, *192*, 5.
- [28] M. C. Bernini, J. C. Garro, E. V. Brusau, G. E. Narda, E. L. Varetti, *J. Mol. Struct.* **2008**, *888*, 113–123.
- [29] S. D. Ross, *Inorganic Infrared and Raman Spectra*, McGraw-Hill, London, **1972**.
- [30] a) J. Fuhrhop, G. Penzlin in *Organic Synthesis, Concepts, Methods, Starting Materials*, 2nd ed., VCH, Weinheim, **1994**; b) E. Block, in *Reactions of Organosulfur Compounds*, Academic Press, New York, **1978**.
- [31] F. Gándara, A. d. Andrés, B. Gómez-Lor, E. Gutiérrez-Puebla, M. Iglesias, M. A. Monge, D. M. Proserpio, N. Snejko, *Cryst. Growth Des.* **2008**, *8*, 378–380.
- [32] T. W. Greene, P. G. M. Wuts in *Protective Groups in Organic Synthesis*, 2nd ed., Wiley, New York, **1991**.
- [33] M. E. Evans, *Carbohydr. Res.* **1972**, *21*, 473.
- [34] T. S. Li, S. H. Li, J. T. Li, H. Z. Li, *J. Chem. Res.* **1997**, 26–27.

- [35] M. J. Ashton, C. Lawrence, J. A. Karlsson, K. A. J. Stuttle, C. G. Newton, B. Y. J. Vacher, S. Webber, M. J. Withnall, *J. Med. Chem.* **1996**, *39*, 4888–4896.
- [36] K. Bauer, D. Garbe, H. Surburg in *Common Fragrances and Flavor Materials*, 2nd ed., VCH, Weinheim, **1990**.
- [37] G. Solladié, *Synthesis* **1981**, 185–196.
- [38] B. S. Lane, K. Burgess, *Chem. Rev.* **2003**, *103*, 2457–2473.
- [39] I. Kostova, N. Peica, W. Kiefer, *J. Raman Spectrosc.* **2007**, *38*, 1–10.
- [40] A. M. Heyns, K. J. Range, *J. Raman Spectrosc.* **1994**, *25*, 855–859.
- [41] a) F. Gándara, J. Perles, N. Snejko, M. Iglesias, B. Gomez-Lor, E. Gutierrez-Puebla, M. A. Monge, *Angew. Chem.* **2006**, *118*, 8166–8169; *Angew. Chem. Int. Ed.* **2006**, *45*, 7998–8001; b) F. Gándara, E. Gutiérrez-Puebla, M. Iglesias, D. M. Proserpio, N. Snejko, M. A. Monge, *Chem. Mater.* **2009**, *121*, 655–661.
- [42] *International Tables for Crystallography, Vol. 4* (Eds.: J. A. Ibers, W. C. Hamilton), Kynoch Press, Birmingham, **1974**.
- [43] Siemens SAINT data collection and procedure software for the SMART system, Siemens Analytical X-Ray Instruments, Inc., Madison (WI), **1995**.
- [44] Siemens SHELXTL, version 5.0, Siemens Analytical X-ray Instruments, Inc., Madison (WI), **1995**.
- [45] E. Dowty, ATOMS for Windows, v. 5.1, a computer program for displaying atomic structure, Shape Software, Kingsport (TN), **1995**.

Received: November 17, 2008

Published online: March 25, 2009